# Synthesis, Giant Dielectric, and Pyroelectric Response of [001]-Oriented $Pr^{3+}$ Doped $Pb(Mg_{1/3}Nb_{2/3})O_3$-$PbTiO_3$ Ferroelectric Nano-Films Grown on Si Substrates

**Changlong Cai [1], Deqiang Zhang [1], Weiguo Liu [1], Jun Wang [2], Shun Zhou [1], Yongming Su [1], Xueping Sun [1] and Dabin Lin [1,*]**

[1] Thin Film and Optical Manufacturing Technology, Key Laboratory of Ministry of Education, Xi'an Technological University, Xi'an 710032, China; cmcwlh@163.com (C.C.); zhangdqiang@163.com (D.Z.); wgliu@163.com (W.L.); zsemail@126.com (S.Z.); yongmingsu@126.com (Y.S.); sunxueping.1988@163.com (X.S.)

[2] Department of Basic Science, Air Force Engineering University, Xi'an 710051, China; wangjun563@163.com

[*] Correspondence: dabinlin@xatu.edu.cn; Tel.: +86-029-8617-3335

check for updates

**Abstract:** The [001]-oriented $Pr^{3+}$ doped $Pb(Mg_{1/3}Nb_{2/3})O_3$-0.30$PbTiO_3$ (Pr-PMN-PT) thin films with a composition near the morphotropic phase boundary (MPB) were synthesized by a sol–gel method. The crystal structure was characterized using X-ray diffraction. It was found that a single perovskite phase was achieved in Pr-PMN-PT thin films annealed at 650 °C for 3 min. The dielectric constant ($\varepsilon_r$) value was 2400 in 2.5% Pr-PMN-PT thin films at room temperature, 110% higher than that of pure PMN-PT samples. Through 2.5% $Pr^{3+}$ doping, remanent polarization ($P_r$) and coercive field ($E_c$) values increased from 11.5 $\mu C/cm^2$ and 35 kV/cm to 17.3 $\mu C/cm^2$ and 63.5 kV/cm, respectively, in PMN-PT thin films. The leakage current densities of pure and 2.5% Pr-PMN-PT thin films were on the order of $1.24 \times 10^{-4}$ $A/cm^2$ and $5.8 \times 10^{-5}$ $A/cm^2$, respectively, at 100 kV/cm. A high pyroelectric coefficient ($p_y$) with a value of 167 $\mu C/m^2 K$ was obtained in 2.5% Pr-PMN-PT thin films on Si substrate, which makes this material suitable for application in infrared detectors.

**Keywords:** thin film; pyroelectric; ferroelectric; dielectric; sol–gel

## 1. Introduction

$Pb(Mg_{1/3}Nb_{2/3})O_3$-$PbTiO_3$ (PMN-PT) bulk piezoelectric materials with compositions near the morphotropic phase boundary have attracted much attention as a candidate piezoelectric material for device application in the fields of microelectromechanical system (MEMS) and nanoelectromechanical systems (NEMS) [1–3]—such as infrared (IR) detectors [4], cantilever-type piezoelectric devices [5,6], multilayer capacitors [7], and ultrasonic transducers [8–10]—due to the high field strain (1.7%) [11], pyroelectric coefficient (~1500 $\mu C/m^2 K$) [12], and longitudinal coupling factor (~95%) [13,14]. Especially for uncooled IR detectors, pyroelectricity is indeed one of the most promising principles. Compared with bulk crystals, thin films have the advantage of low-cost, reduced material consumption, small cell size, energy efficiency, and ease of integration in Si semiconductor technology. For PMN-based bulk crystals, the pure perovskite structure can easily be synthesized using the two-step columbite precursor method [15–17]. On the contrary, the second pyrochlore phase in PMN-PT thin films is related to many factors, for example annealing temperature/time [18], sample thickness [19], excess Pb content [20,21], etc., which restrict the pyroelectric, piezoelectric, and dielectric properties in PMN-PT thin films.

Many methods and approaches—such as radio frequency (RF) magnetron sputtering [22], pulsed laser deposition (PLD) [4], chemical vapor deposition (CVD) [23], chemical solution deposition (CSD) [24], and so forth—have been adopted to fabricate high-quality PMN-PT thin films. Sol–gel processing, a kind of chemical solution deposition, has many advantages that make it suitable for obtaining high-quality PMN-PT thin films on Si substrate for industrial applications [25,26]. Dielectric constants and remanent polarization in slim P-E hysteresis loops were on the order of 1692 and 13.31 $\mu C/cm^2$ respectively in the PMN-0.30PT thin films using sol-gel technology [27]. Recently, a giant pyroelectric response ($-550$ $\mu Cm^{-2}K^{-1}$) driven by the electric field was obtained in $0.68Pb(Mg_{1/3}Nb_{2/3})O_3\text{-}0.32PbTiO_3/Ba_{0.5}Sr_{0.5}RuO_3$ hetero structures grown on [110]-oriented $NdScO_3$ single crystals by pulsed-laser deposition (PLD) [4] indicating good potential for low dimensional pyroelectric devices.

Rare earth elements such as $Er^{3+}$, $La^{3+}$, and so forth have been used to improve the up-conversion photoluminescence in bulk piezoelectric materials [28,29]. Recently, an ultrahigh piezoelectric coefficient ($d_{33}$ = 1500 pC/N) was obtained in Sm-doped PMN-PT polycrystalline [30] based on polar nano-region (PNR) design in relaxor based ferroelectric materials. For $Pb(Zr,Ti)O_3$ (PZT) thin films, the dielectric and piezoelectric properties were improved by La doping [31]. Until now, little research has focused on the pyroelectric or piezoelectric properties of rare earth element-doped relaxor-PT (PMN-PT or PIN-PMN-PT) thin films. With the aim of low cost and high performance materials for MEMS device fabrication, the $Pr^{3+}$ doped PMN-PT thin films were prepared by the sol–gel method at various annealed temperatures and times. The phase structure of the samples was analyzed by X-ray diffraction. Then, the surface morphology of Pr-PMN-PT thin films was measured by scanning electron microscopy, atomic force microscopy, and piezoresponse force microscopy. Finally, dielectric, pyroelectric, and ferroelectric properties of Pr-PMN-PT thin films were investigated.

## 2. Materials and Methods

Before sol–gel processing, a $TiO_2$ diffusion barrier layer was first fabricated by oxidizing the Ti metal layer as follows: Ti films of 60 nm thickness were deposited on $SiO_2/Si$ (100) substrate by DC magnetron sputtering in an Ar gas environment at room temperature. The sputtering power was 175 W. The base vacuum of Ti sputtering was higher than $8 \times 10^{-4}$ Pa. The ratio of $Ar:O_2$ was 90:10. After deposition, the Ti layer was annealed in a rapid thermal processing (RTP) furnace at 700 °C for 1 h. Then, a Pt bottom electrode of 80 nm thickness was deposited on the $TiO_2$ diffusion barrier layer. The sputtering parameters were the same as the Ti metal layer deposition. The sheet resistance was about 2.85 $\Omega/sq$, which was measured by the four probe method.

After that, $Pr^{3+}$ doped $Pb(M_{1/3}Nb_{2/3})O_3$-$0.30PbTiO_3$ (xPr-(1 − x)(PMN-0.30PT), x = 1%, 2%, 2.5%, and 3%) precursor solutions were prepared by the sol–gel method. The lead acetate trihydrate ($Pb(CH_3COO)_2 \cdot 3H_2O$), magnesium acetate tetrahydrate ($Mg(CH_3COO)_2 \cdot 4H_2O$), niobium ethoxide ($Nb(OCH_3CH_2)_5$), tetrabutyl titanate ($Ti(OC_4H_9)_4$), and praseodymium acetyl acetone ($C_{15}H_{21}PrO_6 \cdot xH_2O$) were used as starting materials to synthesize the Pr-PMN-PT sol–gel solution. An additional 20 mol% of lead acetate trihydrate was added to equalize the Pb volatilization and 5 mol% more magnesium acetate tetrahydrate was mixed to boost the production of perovskite phase. Next, 2-methoxyethanol ($C_5H_8O_2$) and glacial acetic acid ($CH_3COOH$) were added as solvent and catalyst respectively. Acetyl acetone ($C_5H_8O_2$) was added as a stabilizer in the Pb-Pr-Mg-Nb-Ti solution. The concentration of the Pr-PMN-PT solution was attenuated to 0.4 mol/L. Then, the Pr-PMN-PT thin films were deposited by spin coating on $Pt/TiO_2/SiO_2/Si$ substrates at 2000 rpm for 9 s before the spin coating was subsequently sped up to 4000 rpm for 20 s. To evaporate the solvent in solution, the sample was dried at 220 °C for 3 min after each deposition and then pyrolyzed at 450 °C for 5 min. Finally, Pr-PMN-PT films were annealed at 600, 650, and 700 °C for 1–5 min in air by RTP at ramp rates +20 °C/s and −5 °C/s respectively. In order to get 500 nm thick film, this entire process was repeated 10 times. For further electric measurement, Au top electrodes were deposited on Pr-PMN-PT samples using magnetron sputtering through a shadow mask with a 1 mm diameter.

The crystalline structure of Pr-PMN-PT thin films was analyzed by X-ray diffraction (XRD) (Shimadzu X-6000, Kyoto, Japan) with Cu-K$\alpha$ radiation in the 2theta range of 20°–60° and a scan step length of 0.02 at room temperature. The surface morphologies of the samples were characterized by a field emission scanning electron microscope (FE-SEM) (ZEISS Gemini SEM 500, Jena, Germany), atomic force microscope (AFM) (Bruker Multimode 8, Billerica, MA, USA), and piezoresponse force microscopy (PFM) (Bruker dimension icon, Billerica, MA, USA). For electric measurement, the samples were all of a pure perovskite phase structure due to the high electric performance. The dielectric properties were measured using an impedance analyzer (HP 4284, Hewlett Packard, Palo Alto, CA, USA) with a precision LCR meter connected to a heating stage (Linkam THMSE 600, Waterfield, UK). The P-E hysteresis loops and leakage current were examined by a standard ferroelectric system (aixACCT TF-2000, Aachen, Germany). The pyroelectric coefficient ($p_y$) was calculated by the equation as below:

$$p_y(T) = \frac{I}{A\frac{dT}{dt}} \left( \mu C/m^2 K \right),$$  (1)

where $I$ is the pyroelectric current, $A$ is the surface area of the samples, and $dT/dt$ is the rate of temperature cooling.

## 3. Results and Discussion

### 3.1. Phase Structure

Avoiding the formation of a pyrochlore phase is a key factor for the synthesis of PMN-PT thin films as the addition of this phase will reduce the piezoelectric and ferroelectric properties of the resulting thin films. In order to restrict the formation of a pyrochlore phase, the annealing conditions for thin film preparation were first investigated. Figure 1a,b show the X-ray diffraction patterns of 2.5% $Pr^{3+}$ doped PMN-0.30PT thin films deposited on $Pt/TiO_2/SiO_2/Si$ substrates annealed at 600 °C, 650 °C, and 700 °C for 2 min. The perovskite phase peaks were observed at 2θ = 22.1°, 31.4°, 38.6°, 45.2°, 50.9°, and 56.0°, corresponding to the (001), (110), (111), (002), (220), and (112) reflections respectively. The pyrochlore phase peak (222) at 2θ = 29.4° was clear for samples annealed at 600 °C and 700 °C and was identified as $Pb_2Nb_2O_7$ by the comparison to JCPDS No. 40-828, which showed the other characteristic diffraction peak at 2θ = 34.1°. Compared to the typical PMN-PT solid solution, the single perovskite structure was obtained at 650 °C, which showed two strong peaks at 2θ = 22.2° and 45.3°, indicating a mainly preferred crystal growth along the $(001)_c$ direction. Figure 1c,d present the phase structure of 2.5% Pr-PMN-PT thin films deposited on $Pt/TiO_2/SiO_2/Si$ substrates annealed at 650 °C for 1 min, 3 min, and 5 min respectively. It was found that 2.5% Pr-PMN-PT thin films were mostly in the perovskite phase with a little pyrochlore phase when annealed for 1 min, which was further crystallized to a single perovskite phase structure after one more minute annealing. However, a peak of the pyrochlore phase was found again in the sample annealed for 5 min, which can be ascribed to the greater lead loss caused by the longer time annealing [19].

The degree of (001) texture in 2.5% Pr-PMN-PT thin film was evaluated by preferred orientation parameter $\alpha_{hkl}$, which can be calculated by the following formula [32]:

$$\alpha_{hkl} = \frac{I_{hkl}}{\sum I_{hkl}},$$  (2)

where $I_{hkl}$ is the relative intensity of the corresponding diffraction peaks (hkl). As shown in Figure 1a,c, $\alpha_{001}$ values are 86.6% and 73.6% in Pr-PMN-PT thin films annealed at 650 °C for 2 and 3 min respectively, presenting the highly (001)-oriented textured structure. The preferred orientation was related to many factors, such as substrate materials [33], growth method, doping elements [31], annealing temperatures [34], and so forth. For Pr-PMN-PT thin films, the nucleation was in random direction at the start of thin film growth on the surface of Pt. With further temperature increases up to 650 °C, the (001) direction became the preferential growth direction.
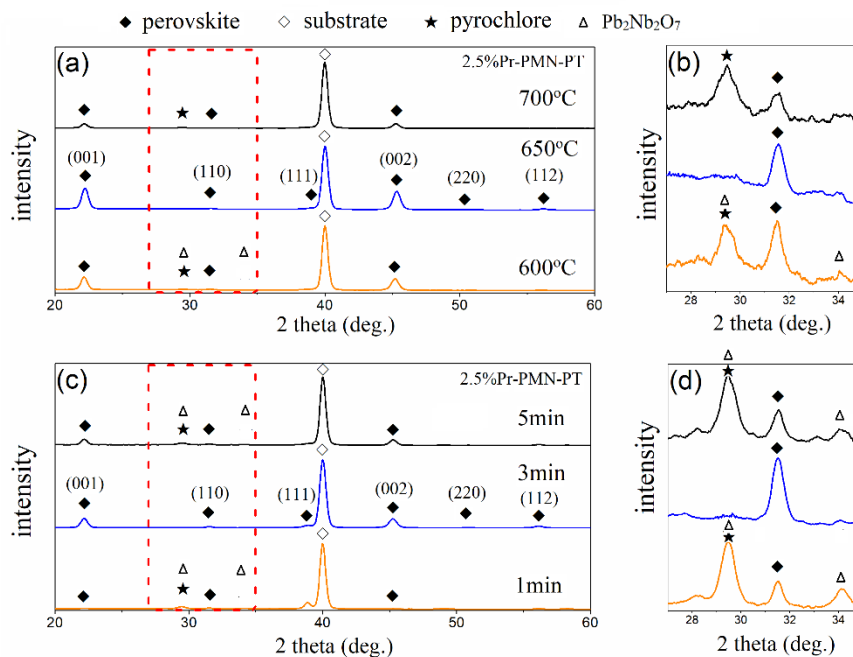
**Figure 1.** XRD patterns of 2.5% $Pr^{3+}$ doped $Pb(Mg_{1/3}Nb_{2/3})O_3$-0.30$PbTiO_3$ (Pr-PMN-PT) thin films as a function of annealing temperatures between 600 °C and 700 °C: (**a,b**); XRD patterns of 2.5% Pr-PMN-PT thin films annealed at 650 °C as a function of annealing times between 1 min and 5 min: (**c,d**).

### 3.2. Surface Morphology and Electric Properties at Room Temperature

Figure 2a,b shows the FE-SEM images of surface and cross-sectional micrographs of Pr-PMN-PT thin films. From these images, it can be seen that the thin films have a dense structure without any cracks. It can further be seen that the quite uniform Pr-PMN-PT, Pt, and $TiO_2$ films are around 450 nm, 80 nm, and 80 nm in thickness respectively, which are in agreement with the values measured by a surface profilometer. Figure 2c presents surface grain size distributions calculated from the image in Figure 2a, showing an average grain size of 100 nm. A typical out-of-plane image with a $3 \times 3 \ \mu m^2$ scan area at the surface of 2.5% Pr-PMN-PT thin films is shown in Figure 2d. The grain size is about 100 nm, in accordance with the FE-SEM observation. However, nano-domains could not be found in the picture, which can be analyzed by macroscale level ferroelectric properties, similar to the results in Ref. [35,36]. The 3D AFM image of 2.5% Pr-PMN-PT thin films is shown in Figure 2e. The root mean square roughness ($R_{rms}$) is about 2.59 nm with a scan area of $2 \times 2 \ \mu m^2$, indicating low interference of electrode contact in electronic measurement. A schematic of the device for further electric investigation is shown in Figure 2f. Two silver wires for electric measurement were bonded to the surface of the Au electrodes.

The dielectric, pyroelectric, and ferroelectric properties in 2.5% Pr-PMN-PT thin films at room temperature are summarized in Table 1. The values of $\varepsilon_r$, $p_y$, and $p_r$ in 2.5% Pr-PMN-PT thin films were on the order of 2400, 167 $\mu C/m^2 K$, and 17.3 $\mu C/cm^2$, showing 110%, 123%, and 50% higher factors respectively than those in pure PMN-PT thin films. Compared with PMN-0.30PT grown by a chemical solution deposition (CSD) method [19], the $\varepsilon_r$ in PMN-0.30PT thin films on Si substrate was lower than that of the sample synthesized on perovskite structure single crystal substrates. A similar tendency of pyroelectric property was found in PMN-0.30PT thin film grown on various substrates. The $p_r$ value in 2.5% Pr-PMN-PT thin films was still higher than that of PMN-0.32PT thin films deposited on $Ba_{0.5}Sr_{0.5}RuO_3$/$NdScO_3$ and $La_{0.5}Sr_{0.5}CoO_3$/$LaAlO_3$ crystals using pulsed laser deposition. In contrast, the $p_y$ value showed an opposite trend, which is attributed to the lattice misfit. Compared with PVDF and normal ferroelectric material, the relaxor-PT thin films showed higher dielectric and pyroelectric properties. In contrast, the response time of the PMN-0.30PT pyroelectric sensor was longer than that of PVDF [37] and $LiTaO_3$ [38].
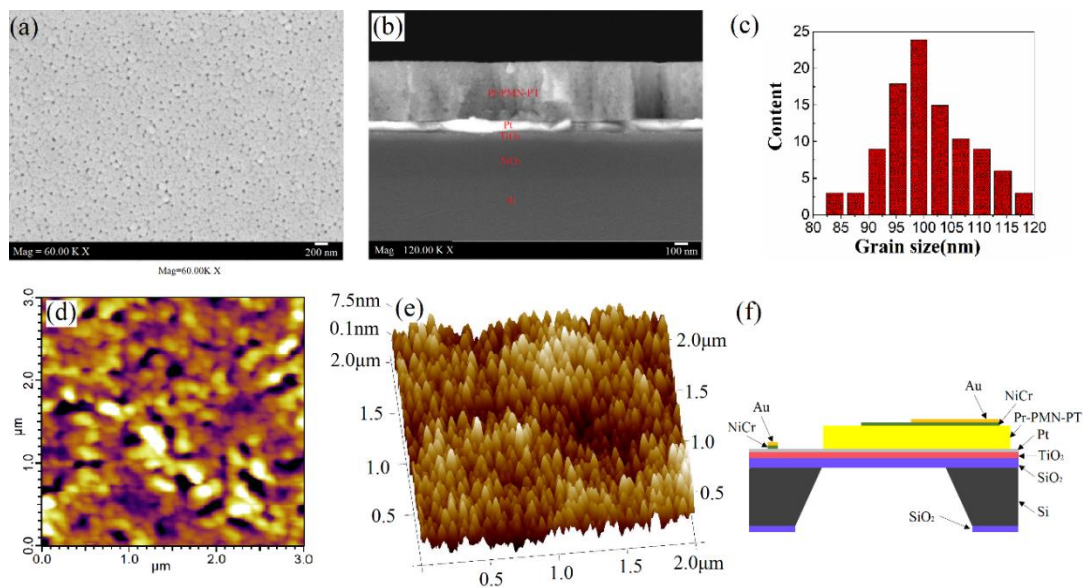
**Figure 2.** (**a**) FE-SEM images of surface morphologies for 2.5% Pr-PMN-PT thin films annealed at 650 °C for 2 min, (**b**) FE-SEM images of cross-section of 2.5% Pr-PMN-PT thin films, (**c**) grain size distributions of 2.5% Pr-PMN-PT thin films, (**d**) 2D piezoresponse force microscope (PFM) images of surface morphologies for 2.5% Pr-PMN-PT thin films, (**e**) 3D atomic force microscope (AFM) images of surface morphologies for 2.5% Pr-PMN-PT thin films, and (**f**) a schematic illustration of the device for electric properties measurement.

**Table 1.** Dielectric, pyroelectric, and ferroelectric properties in (001)-oriented PMN-PT based ferroelectric thin films at room temperature.

| Thin Films | Substrates | Thickness (nm) | Method | $\varepsilon_r$ @1kHz | $\tan\delta$ (%) | $p_y$ ($\mu C/m^2 K$) | $p_r$ ($\mu C/cm^2$) | Reference |
|---|---|---|---|---|---|---|---|---|
| PMN-0.30PT | Pt/TiO$_2$/SiO$_2$/Si | 450 | Sol-gel | 1140 | 3.1 | 75 | 11.5 | This work |
| 2.5%Pr-PMN-0.30PT | Pt/TiO$_2$/SiO$_2$/Si | 450 | Sol-gel | 2400 | 1.5 | 167 | 17.3 | This work |
| PMN-0.30PT | Pt/TiO$_2$/SiO$_2$/Si | 350 | CSD | 1710 | 0.8 | / | / | [20] |
| PMN-0.32PT | Pt/Si/ITO glass | 800 | Sol-gel | 1110 | / | / | 0.55 | [39] |
| PMN-0.30PT | SrRuO$_3$/SrTiO$_3$ | 200 | CSD | ~2600 | ~5 | / | ~13 | [19] |
| PMN-0.32PT | Ba$_{0.5}$Sr$_{0.5}$RuO$_3$/NdScO$_3$ | 150 | PLD | ~1200 | ~7 | −550 | ~8 | [4] |
| PMN-0.32PT | La$_{0.5}$Sr$_{0.5}$CoO$_3$/LaAlO$_3$ | 150 | PLD | ~2500 | ~7 | 160–300 | ~11 | [40] |
| LiNbO$_3$ | SiO$_2$ | $325 \times 10^3$ | / | / | / | 40 | ~50 | [41,42] |
| PVDF | PMMA | $28 \times 10^3$ | / | / | ~5 | 23 | / | [37,43] |

$\varepsilon_r$ dielectric constant, $\tan\delta$ dielectric loss, $p_y$ pyroelectric coefficient, $p_r$ remnant polarization, pulsed-laser deposition (PLD), chemical solution deposition (CSD).

In order to evaluate the Pr$^{3+}$ doping effect in PMN-PT thin films, the elements distribution was measured, as shown in Figure 3, corresponding to the surface micrograph presented in Figure 2a. The Pb, Mg, O, Pr, Nb, Ti, Si, and Pt maps were achieved by performing standardless quantification of the energy dispersive X-ray spectrometry (EDS) signals in the L$\alpha$1 and K$\alpha$1 peaks. From these pictures, it can be seen that the Pb, Mg, Nb, Ti, Si, and Pt elements were homogeneously distributed in the local area. It is interesting to note that the Pr element is mostly distributed along the grain boundaries of thin films, compared to Figure 2a.
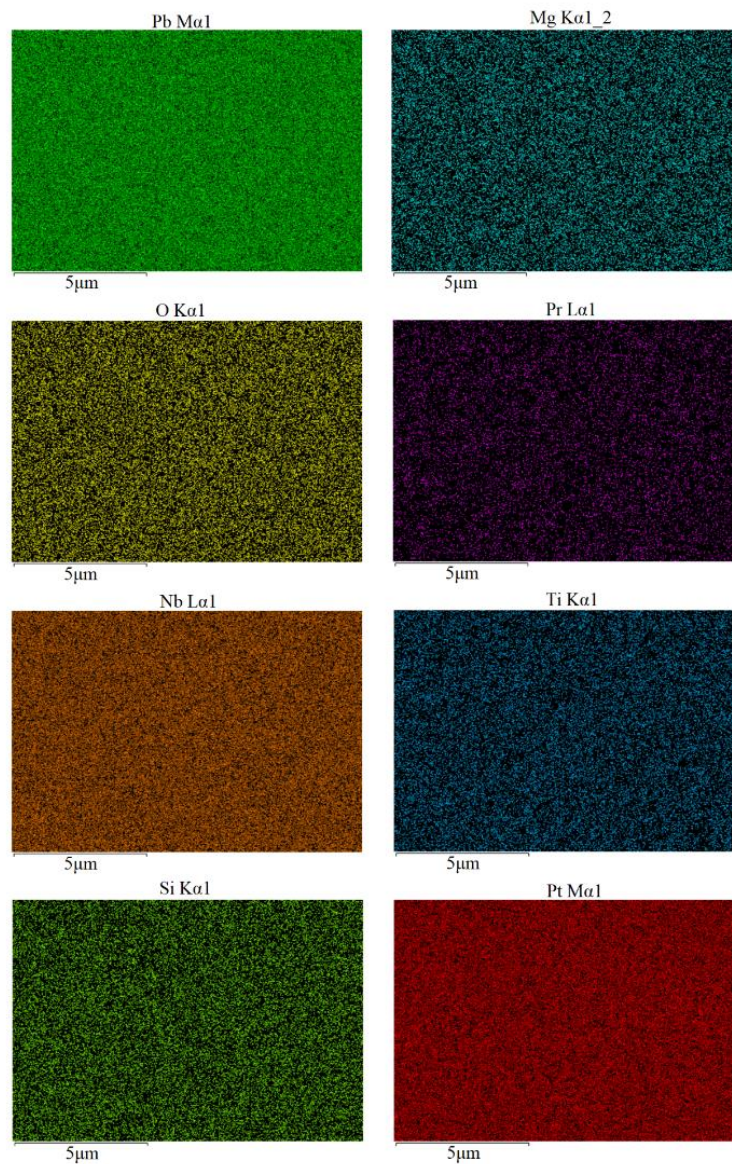
**Figure 3.** Element mapping of 2.5% Pr-PMN-PT thin films annealed at 650 °C for 2 min.

### 3.3. Ferroelectric Properties

Figure 4a presents the ferroelectric properties of Pr-PMN-PT thin films with different $Pr^{3+}$ ratios of 0, 1.5%, and 2.5%. The addition of $Pr^{3+}$ in PMN-PT thin films increased the value of remanent polarization ($P_r$) and coercive field ($E_c$) from 11.5 $\mu C/cm^2$ and 35 kV/cm to 17.3 $\mu C/cm^2$ and 63.5 kV/cm respectively. The leakage current densities of pure and 2.5% Pr-PMN-PT thin films were approximately $1.24 \times 10^{-4}$ $A/cm^2$ and $5.8 \times 10^{-5}$ $A/cm^2$ respectively at 100 kV/cm, as shown in Figure 4b. A donor dopant in PMN-PT samples was poled at the higher electric field due to the higher $E_c$ in Pr-PMN-PT thin films, indicating that the domain structure was easily reoriented owing to the presence of lead vacancies near the grain boundaries [44,45], corresponding to the $Pr^{3+}$ ion distribution shown in Figure 3. Those effects also led to a higher dielectric constant of $Pr^{3+}$ doped compositions compared to the undoped counterpart, as shown in Table 1.
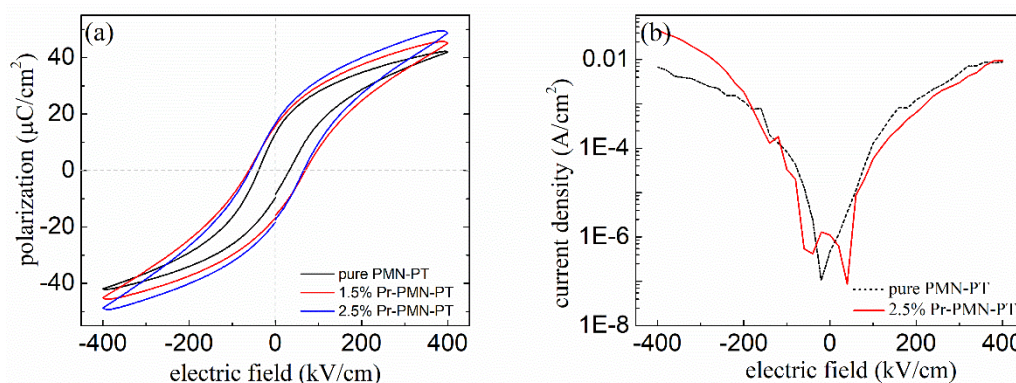
**Figure 4.** (**a**) P-E hysteresis loops for pure PMN-PT and Pr-PMN-PT thin films annealed at 650 °C for 2 min, (**b**) leakage current density dependent on external electric field for pure PMN-PT and 2.5% Pr-PMN-PT thin films.

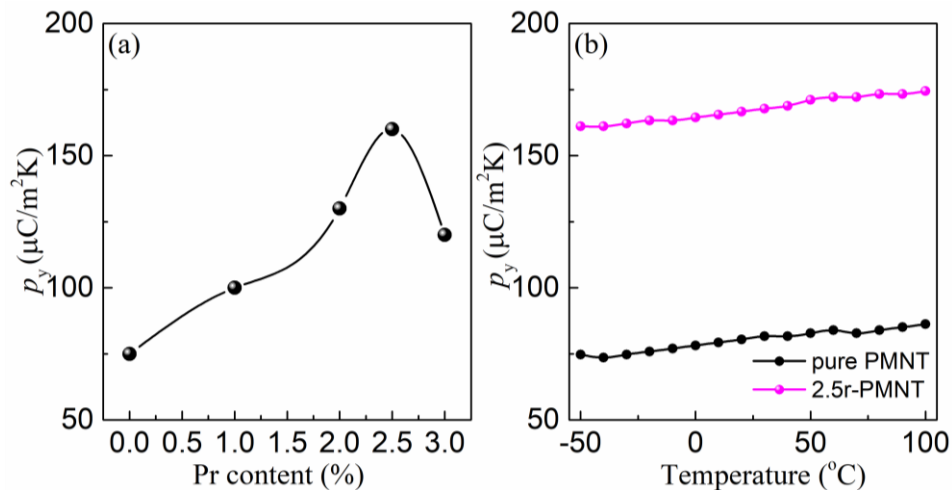*3.4. Temperature Dependent of Dielectric and Pyroelectric Properties*

Figure 5a shows dielectric constant ($\varepsilon_r$) and dielectric loss (tan$\delta$) of Pr-PMN-PT thin films in the frequency range of 20 Hz to 200 kHz at room temperature. We see that the $\varepsilon_r$ value decreased slightly with an increasing frequency, which is induced by the polarization decrease due to charge accumulation at low frequency. Meanwhile, the dielectric loss showed a very quick increase in the range $10^4$–$2 \times 10^5$ Hz, indicating conduction through the electrode surface and grain boundary capacitance interference in poled samples at high frequency. Figure 5b presents the dielectric properties dependent on temperature for Pr-PMN-PT thin film at 100 Hz and 1 kHz. The $\varepsilon_r$ curve presents a broad peak centered at around 100 °C, which corresponds to the diffuse ferroelectric to paraelectric phase transition [10,17]. The value of dielectric loss values is about 1.8% in the temperature range from 25 to 100 °C, which indicates good electrode bonding for further device integrating.
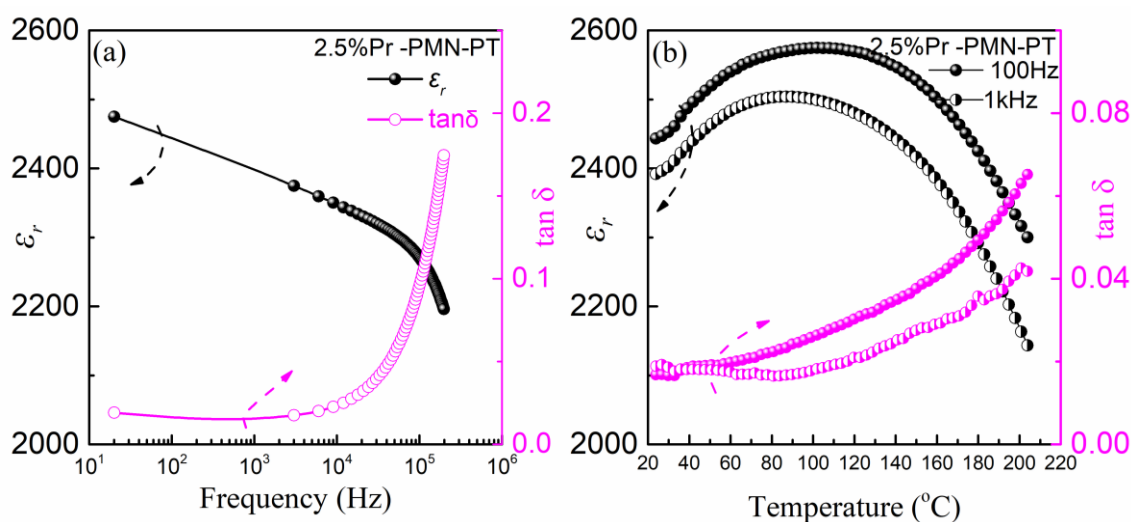


**Figure 5.** (**a**) Dielectric coefficient ($\varepsilon_r$) and dielectric loss (tan$\delta$) as a function of frequency for 2.5% Pr-PMN-PT thin films annealed at 650 °C for 2 min, (**b**) dielectric coefficient and dielectric loss as a function of temperature for 2.5% Pr-PMN-PT thin films at 100 Hz and 1 kHz.

Figure 6a shows the pyroelectric coefficient ($p_y$) measured at room temperature for the obtained PMN-PT thin films as a function of $Pr^{3+}$ doping content. The $p_y$ in the thin films with 2.5% dopant presented the maximum value on the order of 167 $\mu$C/m$^2$K, which is almost a two-fold increase over that of pure PMN-PT thin films, offering a new way for enhancing the pyroelectric performance in relaxor-PT thin films for use in infrared detectors. The temperature dependence of $p_y$ values is

illustrated in Figure 6b. In the temperature range of $-50$–$100\,^{\circ}$C, the pyroelectric coefficient showed a slight fluctuation (~10%), indicating good thermal stability for application in infrared detectors integrated into Si semiconductor devices.



**Figure 6.** (**a**) Pyroelectric coefficient ($p_{\mathrm{y}}$) dependent of Pr content in Pr-PMN-PT thin film annealed at 650 $^{\circ}$C for 2 min; (**b**) pyroelectric coefficient ($p_{\mathrm{y}}$) measured in pure PMN-PT and 2.5% Pr-PMN-PT thin films at temperature between $-50\,^{\circ}$C and $100\,^{\circ}$C.

## 4. Conclusions

The pure and $Pr^{3+}$ doped PMN-PT ferroelectric thin films with a single perovskite structure were prepared by a sol–gel processing and investigated by X-ray diffraction. The microstructure of Pr-PMN-PT samples was characterized by scanning electron microscopy, atomic force microscopy, and piezoresponse force microscopy. The average grain size was about 100 nm. It was found that $Pr^{3+}$ ions were located at the edge of grain boundaries measured by energy dispersive X-ray spectroscopy. For 2.5% $Pr^{3+}$ doping, the dielectric constant, pyroelectric coefficient, and remanent polarization all reached a maximum. Importantly, the dielectric constant in PMN-PT thin films increased from 1140 to 2400 through 2.5% $Pr^{3+}$ doping. Such enhancement was ascribed to the domain wall motion induced by the $Pr^{3+}$ ion distribution around the grain boundary. Finally, this rare earth dopant presents a useful method for developing high performance relaxor-PT thin films for use in energy transducers and photodetectors.

## References

1.  Baek, S.-H.; Rzchowski, M.S.; Aksyuk, V.A. Giant piezoelectricity in PMN-PT thin films: Beyond PZT. *MRS Bull.* **2012**, *37*, 1022–1029. [CrossRef]
2.  Cordero, F. Elastic Properties and Enhanced Piezoelectric Response at Morphotropic Phase Boundaries. *Materials* **2015**, *8*, 5452. [CrossRef] [PubMed]

3.  Lin, D.; Li, Z.; Cheng, Z.Y.; Xu, Z.; Yao, X. Electric-field-induced polarization fatigue of [001]-oriented Pb($Mg_{1/3}Nb_{2/3}$)$O_3$–0.32PbTiO$_3$ single crystals. *Solid State Commun.* **2011**, *151*, 1188–1191. [CrossRef]

4.  Pandya, S.; Wilbur, J.; Kim, J.; Gao, R.; Dasgupta, A.; Dames, C.; Martin, L.W. Pyroelectric energy conversion with large energy and power density in relaxor ferroelectric thin films. *Nat. Mater.* **2018**, *17*, 432. [CrossRef] [PubMed]

5.  Lee, S.H.; Jeong, C.K.; Hwang, G.-T.; Lee, K.J. Self-powered flexible inorganic electronic system. *Nano Energy* **2015**, *14*, 111–125. [CrossRef]

6.  Zhang, S.; Li, F.; Lee, H.J.; Lin, D.; Shrout, T.R.; Luo, J.; Meyer, R.J. Evaluation of PMN-PT based crystals for various applications. In Proceedings of the 2011 International Symposium on Applications of Ferroelectrics (ISAF/PFM) and 2011 International Symposium on Piezoresponse Force Microscopy and Nanoscale Phenomena in Polar Materials, Vancouver, BC, Canada, 24–27 July 2011; pp. 1–4.

7.  Moya, X.; Defay, E.; Mathur, N.D.; Hirose, S. Electrocaloric effects in multilayer capacitors for cooling applications. *MRS Bull.* **2018**, *43*, 291–294. [CrossRef]

8.  Zhang, T.; Ou-Yang, J.; Yang, X.; Zhu, B. Transferred PMN-PT Thick Film on Conductive Silver Epoxy. *Materials* **2018**, *11*, 1621. [CrossRef] [PubMed]

9.  Chen, Y.; Lam, K.-H.; Zhou, D.; Yue, Q.; Yu, Y.; Wu, J.; Qiu, W.; Sun, L.; Zhang, C.; Luo, H.; et al. High Performance Relaxor-Based Ferroelectric Single Crystals for Ultrasonic Transducer Applications. *Sensors* **2014**, *14*, 13730. [CrossRef] [PubMed]

10. Lin, D.; Lee, H.J.; Zhang, S.; Li, F.; Li, Z.; Xu, Z.; Shrout, T.R. Influence of domain size on the scaling effects in Pb($Mg_{1/3}Nb_{2/3}$)$O_3$–PbTiO$_3$ ferroelectric crystals. *Scripta Mater.* **2011**, *64*, 1149–1151. [CrossRef] [PubMed]

11. Park, S.-E.; Shrout, T.R. Ultrahigh strain and piezoelectric behavior in relaxor based ferroelectric single crystals. *J. Appl. Phys.* **1997**, *82*, 1804–1811. [CrossRef]

12. Choi, S.W.; Shrout, R.T.R.; Jang, S.J.; Bhalla, A.S. Dielectric and pyroelectric properties in the Pb($Mg_{1/3}Nb_{2/3}$)$O_3$-PbTiO$_3$ system. *Ferroelectrics* **1989**, *100*, 29–38. [CrossRef]

13. Li, F.; Zhang, S.; Xu, Z.; Chen, L.-Q. The Contributions of Polar Nanoregions to the Dielectric and Piezoelectric Responses in Domain-Engineered Relaxor-PbTiO$_3$ Crystals. *Adv. Funct. Mater.* **2017**, *27*, 1700310. [CrossRef]

14. Kazys, R.; Sliteris, R.; Sestoke, J. Air-Coupled Ultrasonic Receivers with High Electromechanical Coupling PMN-32%PT Strip-Like Piezoelectric Elements. *Sensors* **2017**, *17*, 2365. [CrossRef] [PubMed]

15. Swartz, S.L.; Shrout, T.R. Fabrication of perovskite lead magnesium niobate. *Mater. Res. Bull.* **1982**, *17*, 1245–1250. [CrossRef]

16. Lin, D.; Li, Z.; Li, F.; Xu, Z.; Yao, X. Characterization and piezoelectric thermal stability of PIN–PMN–PT ternary ceramics near the morphotropic phase boundary. *J. Alloys Compd.* **2010**, *489*, 115–118. [CrossRef]

17. Lin, D.; Li, Z.; Zhang, S.; Xu, Z.; Yao, X. Electric-field and temperature induced phase transitions in Pb($Mg_{1/3}Nb_{2/3}$)$O_3$–0.3PbTiO$_3$ single crystals. *J. Appl. Phys.* **2010**, *108*, 034112. [CrossRef]

18. Shen, B.; Wang, J.; Pan, H.; Chen, J.; Wu, J.; Chen, M.; Zhao, R.; Zhu, K.; Qiu, J. Effects of annealing process and the additive on the electrical properties of chemical solution deposition derived 0.65Pb($Mg_{1/3}Nb_{2/3}$)$O_3$–0.35PbTiO$_3$ thin films. *J. Mater. Sci. Mater. Electron.* **2018**, *29*, 16997–17002. [CrossRef]

19. Keech, R.; Morandi, C.; Wallace, M.; Esteves, G.; Denis, L.; Guerrier, J.; Johnson-Wilke, R.L.; Fancher, C.M.; Jones, J.L.; Trolier-McKinstry, S. Thickness-dependent domain wall reorientation in 70/30 lead magnesium niobate-lead titanate thin films. *J. Am. Ceram. Soc.* **2017**, *100*, 3961–3972. [CrossRef]

20. Keech, R.; Shetty, S.; Wang, K.; Trolier-McKinstry, S. Management of Lead Content for Growth of {001}-Oriented Lead Magnesium Niobate-Lead Titanate Thin Films. *J. Am. Ceram. Soc.* **2016**, *99*, 1144–1146. [CrossRef]

21. Borman, T.M.; Zhu, W.; Wang, K.; Ko, S.W.; Mardilovich, P.; Trolier-McKinstry, S.E. Effect of lead content on the performance of niobium-doped {100} textured lead zirconate titanate films. *J. Am. Ceram. Soc.* **2017**, *100*, 3558–3567. [CrossRef]

22. Herdier, R.; Detalle, M.; Jenkins, D.; Soyer, C.; Remiens, D. Piezoelectric thin films for MEMS applications—A comparative study of PZT, 0.7PMN-0.3PT and 0.9PMN-0.1PT thin films grown on Si by r.f. magnetron sputtering. *Sens. Actuators A Phys.* **2008**, *148*, 122–128. [CrossRef]

23. Yutaka, T.; Kosuke, S.; Hiroshi, T.; Kunisaburo, T. Preparation of Lead Magnesium Niobate Titanate Thin Films by Chemical Vapor Deposition. *Jpn. J. Appl. Phys.* **1995**, *34*, 5083.

24. Keech, R.; Shetty, S.; Kuroda, M.A.; Liu, X.H.; Martyna, G.J.; Newns, D.M.; Trolier-McKinstry, S. Lateral scaling of $Pb(Mg_{1/3}Nb_{2/3})O_3$-$PbTiO_3$ thin films for piezoelectric logic applications. *J. Appl. Phys.* **2014**, *115*, 234106. [CrossRef]

25. Kim, Y.-H.; Heo, J.-S.; Kim, T.-H.; Park, S.; Yoon, M.-H.; Kim, J.; Oh, M.S.; Yi, G.-R.; Noh, Y.-Y.; Park, S.K. Flexible metal-oxide devices made by room-temperature photochemical activation of sol–gel films. *Nature* **2012**, *489*, 128. [CrossRef] [PubMed]

26. Karataş, Ş.; El-Nasser, H.M.; Al-Ghamdi, A.A.; Yakuphanoglu, F. High Photoresponsivity Ru-doped ZnO/p-Si Heterojunction Diodes by the Sol-gel Method. *Silicon* **2018**, *10*, 651–658. [CrossRef]

27. Zhou, D.; Sun, H.; Liu, X.; Sui, H.; Guo, Q.; Liu, P.; Ruan, Y. Effects of annealing temperature on structure and electrical properties of sol-gel derived 0.65PMN-0.35PT thin film. *Ceram. Int.* **2017**, *43*, 5901–5906. [CrossRef]

28. Yao, Y.; Luo, L.; Li, W.; Zhou, J.; Wang, F. An intuitive method to probe phase structure by upconversion photoluminescence of $Er^{3+}$ doped in ferroelectric $Pb(Mg_{1/3}Nb_{2/3})O_3$-$PbTiO_3$. *Appl. Phys. Lett.* **2015**, *106*, 082906. [CrossRef]

29. Yang, M.; Long, S.; Yang, X.; Lin, S.; Zhu, Y.; Ma, D.; Wang, B. Temperature-Dependent and Threshold Behavior of $Sm^{3+}$ Ions on Fluorescence Properties of Lithium Niobate Single Crystals. *Materials* **2018**, *11*, 2058. [CrossRef] [PubMed]

30. Li, F.; Lin, D.; Chen, Z.; Cheng, Z.; Wang, J.; Li, C.; Xu, Z.; Huang, Q.; Liao, X.; Chen, L.-Q.; et al. Ultrahigh piezoelectricity in ferroelectric ceramics by design. *Nat. Mater.* **2018**, *17*, 349. [CrossRef] [PubMed]

31. Yang, L.; Zheng, D.-Y.; Guo, K.-X.; Zhao, W.-N.; Peng, Z.-H.; Peng, G.-G.; Zhou, T. Mechanism of grain growth and excellent polarization, dielectric relaxtion of $La^{3+}$, $Nd^{3+}$ modified PZT nano-films prepared by sol–gel technique. *J. Mater. Sci. Mater. Electron.* **2018**, *29*, 18011–18019. [CrossRef]

32. Feng, M.; Wang, W.; Ke, H.; Rao, J.C.; Zhou, Y. Highly (111)-oriented and pyrochlore-free PMN–PT thin films derived from a modified sol–gel process. *J. Alloys Compd.* **2010**, *495*, 154–157. [CrossRef]

33. Gabor, U.; Spreitzer, M.; Uršič, H.; Tchernychova, E.; Samardžija, Z.; Wu, W.J.; Suvorov, D. Structural peculiarities of $0.67Pb(Mg_{1/3}N_{b2/3})O_3$–$0.33PbTiO_3$ thin films grown directly on $SrTiO_3$ substrates. *J. Eur. Ceram. Soc.* **2018**, *38*, 4453–4462. [CrossRef]

34. Batra, V.; Kotru, S. Temperature-controlled-orientation dependence of electrical properties of $Pb_{0.95}La_{0.05}Zr_{0.46}Ti_{0.54}O_3$ thin films. *J. Vac. Sci. Technol. B* **2018**, *36*, 052908. [CrossRef]

35. Detalle, M.; Ferri, A.; Da Costa, A.; Desfeux, R.; Soyer, C.; Rémiens, D. Nanoscale study by piezoresponse force microscopy of relaxor $0.7Pb(Mg_{1/3}Nb_{2/3})O_3$–$0.3PbTiO_3$ and $0.9Pb(Mg_{1/3}Nb_{2/3})O_3$–$0.1PbTiO_3$ thin films grown on platinum and $LaNiO_3$ electrodes. *Thin Solid Films* **2010**, *518*, 4670–4674. [CrossRef]

36. Saranya, D.; John, N.S.; Parui, J.; Krupanidhi, S.B. Studies on Field Dependent Domain Structures in Multi-Grained $0.85PbMg_{1/3}Nb_{2/3}O_3$–$0.15PbTiO_3$ Thin Films by Scanning Force Microscopy. *Integr. Ferroelectr.* **2012**, *134*, 39–47. [CrossRef]

37. Pullano, S.; Mahbub, I.; Islam, S.; Fiorillo, A. PVDF Sensor Stimulated by Infrared Radiation for Temperature Monitoring in Microfluidic Devices. *Sensors* **2017**, *17*, 850. [CrossRef] [PubMed]

38. Abdullah, K.A.; Batal, M.A.; Hamdan, R.; Khalil, T.; Salame, C. Noise effect on performance of IR PVDF pyroelectric detector. *AIP Conf. Proc.* **2018**, *1968*, 030079. [CrossRef]

39. Goel, T.C.; Kumar, P.; James, A.R.; Prakash, C. Processing and Dielectric Properties of Sol-Gel Derived PMN-PT (68:32) Thin Films. *J. Electroceram.* **2004**, *13*, 503–507. [CrossRef]

40. Wang, J.; Wong, K.H.; Chan, H.L.W.; Choy, C.L. Composition control and electrical properties of PMN-PT thin films around the morphotropic boundary. *Appl. Phys. A* **2004**, *79*, 551–556. [CrossRef]

41. Savage, A. Pyroelectricity and Spontaneous Polarization in LiNbO3. *J. Appl. Phys.* **1966**, *37*, 3071–3072. [CrossRef]

42. Brick, D.; Emre, E.; Grossmann, M.; Dekorsy, T.; Hettich, M. Picosecond Photoacoustic Metrology of $SiO_2$ and $LiNbO_3$ Layer Systems Used for High Frequency Surface-Acoustic-Wave Filters. *Appl. Sci.* **2017**, *7*, 822. [CrossRef]

43. Chang, H.H.S.; Huang, Z. Laminate composites with enhanced pyroelectric effects for energy harvesting. *Smart Mater. Struct.* **2010**, *19*, 065018. [CrossRef]

44. Lin, D.; Li, Z.; Li, F.; Zhang, S. Direct observation of domain wall motion and novel dielectric loss in 0.23Pb(In$_{1/2}$Nb$_{1/2}$)O$_3$–0.42Pb(Mg$_{1/3}$Nb$_{2/3}$)O$_3$–0.35PbTiO$_3$ crystals. *CrystEngComm* **2013**, *15*, 6292–6296. [CrossRef]

45. Dabin, L.; Zhenrong, L.; Zhuo, X.; Xi, Y. The polarization fatigue behavior in Pb(Mg$_{1/3}$Nb$_{2/3}$)O$_3$-0.32PbTiO$_3$ single crystals. *J. Phys. Conf. Ser.* **2009**, *152*, 012088.